Chinese Journal of Chemical Engineering 69 (2024) 135–142

Contents lists available at ScienceDirect

Chinese Journal of Chemical Engineering

journal homepage: www.elsevier.com/locate/CJChE

Full Length Article

Effect of solvent on the initiation mechanism of living anionic polymerization of styrene: A computational study

Shen Li [1], Yin-Ning Zhou [2,*], Zhong-Xin Liu [1,*], Zheng-Hong Luo [2,*]

[1] School of Chemical Engineering and Technology, Hainan University, Haikou 570228, China
[2] Department of Chemical Engineering, School of Chemistry and Chemical Engineering, State Key Laboratory of Metal Matrix Composites, Shanghai Jiao Tong University, Shanghai 200240, China

ARTICLE INFO

Article history:
Received 10 October 2023
Received in revised form
23 January 2024
Accepted 24 January 2024
Available online 8 February 2024

Keywords:
Living anionic polymerization
Solvent effect
Reaction kinetics
Computational chemistry
Mathematical modeling
Kinetic modeling

ABSTRACT

For living anionic polymerization (LAP), solvent has a great influence on both reaction mechanism and kinetics. In this work, by using the classical butyl lithium-styrene polymerization as a model system, the effect of solvent on the mechanism and kinetics of LAP was revealed through a strategy combining density functional theory (DFT) calculations and kinetic modeling. In terms of mechanism, it is found that the stronger the solvent polarity, the more electrons transfer from initiator to solvent through detailed energy decomposition analysis of electrostatic interactions between initiator and solvent molecules. Furthermore, we also found that the stronger the solvent polarity, the higher the monomer initiation energy barrier and the smaller the initiation rate coefficient. Counterintuitively, initiation is more favorable at lower temperatures based on the calculated results of ΔG_{TS}. Finally, the kinetic characteristics in different solvents were further examined by kinetic modeling. It is found that in benzene and *n*-pentane, the polymerization rate exhibits first-order kinetics. While, slow initiation and fast propagation were observed in tetrahydrofuran (THF) due to the slow free ion formation rate, leading to a deviation from first-order kinetics.

1. Introduction

Since Szwarc first introduced the concept of living anionic polymerization (LAP) [1], a large number of well-defined polymers have been synthesized by LAP [2,3] as well as other derived controlled polymerization technologies [4,5]. In addition, precise design and control of chain microstructure is also achievable by combining LAP with continuous reaction process, *e.g.*, in continuous stirred tank [6], tubular [7], and loop reactors [8]. From the perspective of reaction mechanism, polymerization is initiated to form anionic active species that undergo chain propagation without termination and chain transfer [9,10]. Of all the external conditions, solvent plays a crucial role in affecting the mechanism and kinetics of LAP.

Mechanistically, the effect of solvent on both externally regulated initiation [11] and traditional initiation mechanisms is complicated [12–15]. Several decades ago, the mechanism of anionic polymerization of styrene (St) in hydrocarbon solvents as well as in tetrahydrofuran (THF) was initially studied by Worsfold *et al.* [16,17]. However, theoretical calculation study on the mechanism of St anionic polymerization is rare. Recently, Morita and van Beylen [18] and Takagi *et al.* [19] investigated the mechanism of LAP of St in cyclohexane and THF, respectively, through density functional theory (DFT) calculations and the most probable pathway for the reaction to occur was identified based on the transition state energy. Nevertheless, the interaction between solvent and initiator has not been involved in previous investigations [18,19].

It is known that the kinetics of LAP can be significantly affected by the polarity of solvents [20,21]. A few decades ago, O'Driscoll and Tobolsky [22] studied the polymerization kinetics of St in benzene and showed that it follows first-order kinetic characteristics; in addition, they also found that the addition of THF accelerates the polymerization. In terms of the effect of counter-ions (Na^+, K^+, Rb^+, Cs^+) in various solvents, *Laflair et al.* [23] studied the polymerization rate using tetraphenylborates (*i.e.*, N_aBPh_4, $KBPh_4$, R_bBPh_4, $CsBPh_4$) and found that in weakly polar solvents, the polymerization rate increases with the increase in counter-ion radius. By contrast, in polar solvents, the change in the counter-ion radius has little effect. In addition, several initiators (*e.g.*, butyl lithium, BuLi)

* Corresponding authors.
E-mail addresses: zhouyn@sjtu.edu.cn (Y.-N. Zhou), liuzhongxin@hainanu.edu.cn (Z.-X. Liu), luozh@sjtu.edu.cn (Z.-H. Luo).

https://doi.org/10.1016/j.cjche.2024.01.007
1004-9541/

have different forms of association in different solvents [24–27]. To better understand polymerization kinetic behaviors, kinetic modeling has been proven to be an enabling tool [5,28,29]. One key point needed to be clear is that the predictive performance of a kinetic model is usually related to the reliability of kinetic parameters [5,28,30]. In this regard, quantum chemical calculations can provide more reliable intrinsic/chemical rate coefficients [30–32].

In this work, computational studies of LAP of St in three representative solvents, *i.e.*, benzene, *n*-pentane, and THF, are carried out to probe the origin of the solvent effect on the initiation mechanism. The dominant mechanistic pathways and the role of different solvents in the polymerization reactions are revealed by DFT calculations. Given the solvent-dependent initiation mechanism, the rate coefficients of forward and backward reactions of the association-dissociation equilibrium of initiator in different solvents, as well as the ion-pair propagation rate coefficient are calculated. Additionally, kinetic modeling of LAP with different initiation mechanisms is conducted with experimental data validation. This work deepens the understanding of the mechanism and kinetics of LAP under different solvents.

2. Computational Methods

2.1. DFT calculation methods

All DFT calculations were performed using the Gaussian 16 program package at the M06-2X/def2tzvp//B3LYP-D3/6-31+g (d, p) level [33]. Solvent effect was explored using the Solvation model based on Density (SMD) [34].

Before calculating a thermodynamic quantity, the raw harmonic frequencies are multiplied by three correction factors (ZPE = 0.963, $H(T) - H(0) = 1.0463$, $S(T) = 1.0554$). In addition, Grimme's quasi rigid-rotor harmonic oscillator (QRRHO) model was applied in the shermo program to take into account the errors due to low-frequency vibrations [35,36].

Reaction rate coefficients were calculated by the modified Eyring transition state theory (TST) (Eqs. (1)–(6)) [37,38]. Electrostatic potentials and intermolecular interactions were performed using the Multiwfn and VMD software packages [39,40]. The sobEDAw method was used for energy decomposition analysis [41].

Eyring's TST:

$$k^{\mathrm{TST}} = \sigma\kappa \frac{k_{\mathrm{B}}T}{h} \mathrm{e}^{-\Delta G^{0,\neq}/(k_{\mathrm{B}}T)} \tag{1}$$

Truhlar formulas (modified TST):

$$\kappa(T) \cong \frac{\frac{\pi\beta}{\alpha}}{\sin\left(\frac{\pi\beta}{\alpha}\right)} + \frac{\beta}{\beta-\alpha}\mathrm{e}^{(\beta-\alpha)V_0},\ \alpha > \beta \tag{2}$$

$$\kappa(T) = \alpha V_0 = \beta V_0,\ \alpha = \beta \tag{3}$$

$$\kappa(T) \cong \frac{\beta}{\beta-\alpha}\{\exp[(\beta-\alpha)V_0] - 1\},\ \alpha < \beta \tag{4}$$

$$\alpha = \frac{2\pi}{h\nu^{\ddagger}} \tag{5}$$

$$\beta = \frac{1}{k_{\mathrm{B}}T} \tag{6}$$

where σ is the degeneracy of the reaction path, κ is the transmission coefficient of tunneling effect, $\nu^{\ddagger}$ is the virtual frequency of transition state (TS), $k_{\mathrm{B}} = 1.381 \times 10^{-23}\ \mathrm{J\cdot K^{-1}}$, $h = 6.626 \times 10^{-34}\ \mathrm{J\cdot s}$, $N_{\mathrm{A}} = 6.023 \times 10^{23}$.

2.2. Kinetic modeling process

Kinetic models for the systems using three representative solvents were established based on the method of moments, which have been well demonstrated in free radical polymerization systems [42–46]. The moment equations were solved numerically by using the Matlab2022a program package. According to the mechanistic reaction pathways of LAP in the three solvents recognized by DFT-assisted calculations (Fig. S1 see Supplementary Material), intrinsic rate coefficient of each elementary reaction was calculated by Eqs. (1)–(6), as summarized in Table 1. It should be noted that the available elementary reactions are written down referring to Ref. [16] and are supported by the DFT herein. Since the initiator BuLi may exist in different configurations of aggregates in solvents, to simplify the calculations, the configuration with the lowest energy was selected (Fig. S2), respectively. Accordingly, the kinetic equations were derived for all species, as shown in Table S1. Definitions of moments for macromolecular species and the corresponding differential moment equations are listed in Tables S2–S6.

3. Results and Discussion

3.1. Interaction analysis between initiator and solvent

To clarify the effect of solvent on the initiation mechanism, weak interactions between initiator and different solvents were analyzed by energy decomposition analysis (EDA), as shown in Fig. 1. It can be found that total weak interaction energy ΔE_{int} (Eq. (7)) between solvent and initiator decreases with an increase in solvent polarity. After energy decomposition, it is found that the largest negative contribution to the ΔE_{int} in benzene and THF is the electrostatic interaction energy ΔE_{els}, which is due to the mutual attraction of positive and negative charges in different fragments. ΔE_{els} in THF is as low as $-73.61\ \mathrm{kcal\cdot mol^{-1}}$ ($1\ \mathrm{kcal\cdot mol^{-1}} = 4.18\ \mathrm{kJ\cdot mol^{-1}}$, Fig. 1(c)), which is much lower than that for benzene and *n*-pentane systems. This is due to the mutual attraction between the oxygen atom (lone electron pair with a negative charge) in THF and the lithium atom (with a positive charge) in BuLi, leading to a reduction in the ΔE_{int}.

$$\Delta E_{\mathrm{int}} = \Delta E_{\mathrm{els}} + \Delta E_{\mathrm{xrep}} + \Delta E_{\mathrm{orb}} + \Delta E_{\mathrm{disp}} \tag{7}$$

where ΔE_{int} ($\mathrm{kcal\cdot mol^{-1}}$) represents the total weak interaction energy of the initiator and solvent; ΔE_{els} ($\mathrm{kcal\cdot mol^{-1}}$) is electrostatic interaction energy; ΔE_{xrep} ($\mathrm{kcal\cdot mol^{-1}}$) is exchange-repulsion energy (including scaled DFT correlation); ΔE_{orb} ($\mathrm{kcal\cdot mol^{-1}}$) is orbital interaction energy; ΔE_{disp} ($\mathrm{kcal\cdot mol^{-1}}$) is dispersion interaction energy.

Moreover, negative contributions to the ΔE_{int} also include orbital interaction energy ΔE_{orb} and dispersion interaction energy ΔE_{disp}, which are relatively small. Finally, the only positive contribution to ΔE_{int} is exchange-repulsion energy ΔE_{xrep}, the value of which is determined by the overlap of electron orbitals between different fragments. Overall, the dominant reason for the lower interaction energy in the solvents with stronger polarity is attributed to the attraction of positive and negative charges between initiator and solvent.

Analysis of electrostatic potential (ESP) and intermolecular interactions provides insight into the molecular properties of the complexes of BuLi and different solvents. When comparing the distribution of ESP on the van der Waals (vdW) surfaces, it is observed that the electrostatic potential of BuLi in THF has a relatively lower negative charge density of $-36.8\ \mathrm{kcal\cdot mol^{-1}}$, compared

Table 1
Elementary reactions and rate coefficients in LAP of St

Entry		Equations	Rate coefficients at 298.15 K[①]	
I (Benzene)	Initiation	$(BuLi)_6 \xrightarrow{k_1} 6\ BuLi$	7.6×10^5	DFT[②]
		$6\ BuLi \xrightarrow{k_{-1}} (BuLi)_6$	7.7×10^5	DFT[②]
		$BuLi + M \xrightarrow{k_{in}} Bu(M)_1^- Li^+$	1.8	DFT[③]
	Equilibrium	$[Bu(M)_n^- Li^+]_2 \xrightarrow{k_a} 2\ Bu(M)_n^- Li^+$	1.3×10^8	DFT[②]
		$2\ Bu(M)_n^- Li^+ \xrightarrow{k_{da}} [Bu(M)_n^- Li^+]_2$	1.1×10^{10}	DFT[②]
	Propagation	$Bu(M)_n^- Li^+ + M \xrightarrow{k_{pi}} Bu(M)_{n+1}^- Li^+$	5.1	DFT[④]
II (*n*-Pentane)	Initiation	$(BuLi)_4 \xrightarrow{k_1} 4\ BuLi$	1.5×10^{11}	DFT[②]
		$4\ BuLi \xrightarrow{k_{-1}} (BuLi)_4$	1.6×10^{11}	DFT[②]
		$BuLi + M \xrightarrow{k_{in}} Bu(M)_1^- Li^+$	3.7	DFT[③]
	Equilibrium	$[Bu(M)_n^- Li^+]_2 \xrightarrow{k_a} 2\ Bu(M)_n^- Li^+$	4.1×10^8	DFT[②]
		$2\ Bu(M)_n^- Li^+ \xrightarrow{k_{da}} [Bu(M)_n^- Li^+]_2$	2.1×10^{10}	DFT[②]
	Propagation	$Bu(M)_n^- Li^+ + M \xrightarrow{k_{pi}} Bu(M)_{n+1}^- Li^+$	6.7	DFT[④]
III (THF)	Initiation	$BuLi + M \xrightarrow{k_{in}} Bu(M)_1^- Li^+$	3.0×10^{-1}	DFT[③]
	Equilibrium	$Bu(M)_n^- Li^+ \xrightarrow{k_a} Bu(M)_n^- + Li^+$	2.2×10^5	DFT[②]
		$Bu(M)_n^- + Li^+ \xrightarrow{k_{da}} Bu(M)_n^- Li^+$	4.7×10^7	DFT[②]
	Propagation	$Bu(M)_n^- Li^+ + M \xrightarrow{k_{pi}} Bu(M)_{n+1}^- Li^+$	2.2	DFT[④]
		$Bu(M)_n^- + M \xrightarrow{k_p} Bu(M)_{n+1}^-$	6.1×10^4	DFT[④]

[①] The units for rate coefficients k_1 and k_a are in terms of s^{-1}, k_{-1} in benzene and *n*-pentane are $L^5 \cdot mol^{-5} \cdot s^{-1}$ and $L^3 \cdot mol^{-3} \cdot s^{-1}$ respectively, others are $L \cdot mol^{-1} \cdot s^{-1}$.
[②] Corresponding to chemical processes without transition states, the value of k is approximated by substituting the Gibbs free energy of the relaxed scan and the tunneling coefficient $\kappa = 1$ into Eqs. (1)–(6).
[③] Corresponding to chemical processes with transition states, the calculated Gibbs free energies and tunneling coefficients κ, are substituted into Eqs. (1)–(6) to obtain the k values.
[④] To simplify the calculations, the propagation rate coefficient for the second monomer was used as an approximation [47,48]. Comparison between the calculated rate coefficients and literature values [16,17] shows a very small difference, proving the reliable results (Table S7).

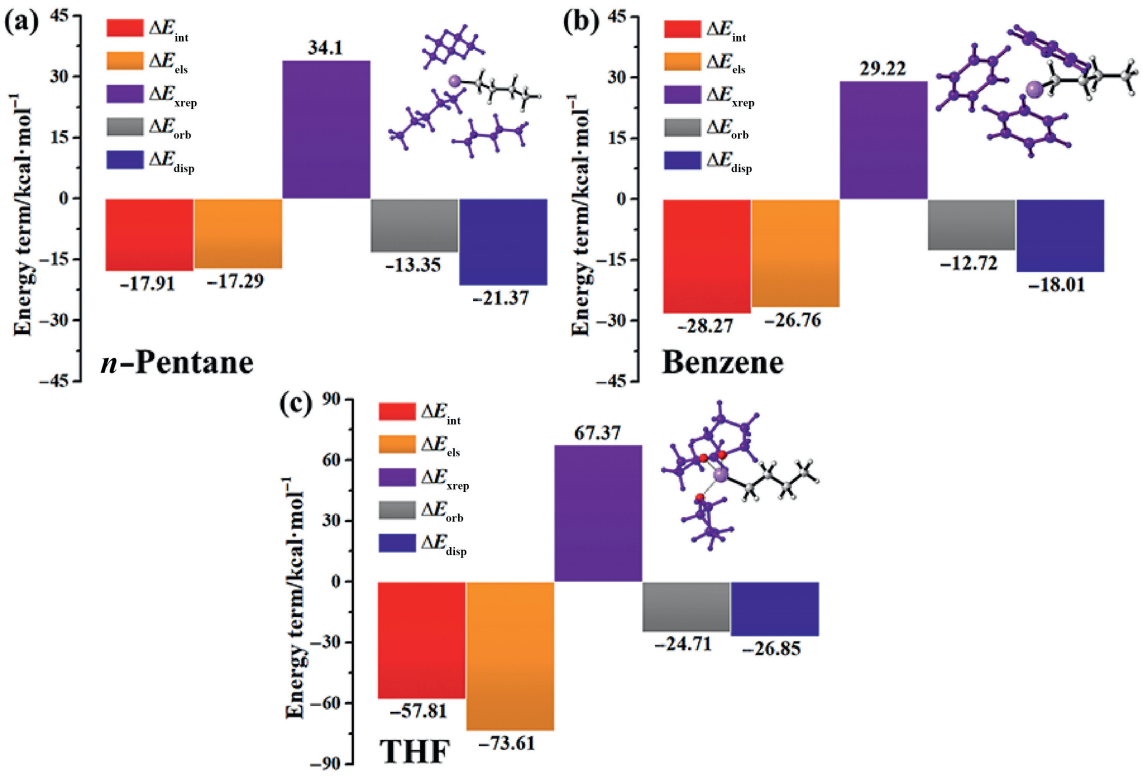

Fig. 1. Energy decomposition analysis (EDA) between BuLi (Bu = C_4H_9) and different solvents: (a) BuLi in *n*-pentane, (b) BuLi in benzene, (c) BuLi in THF.

to −33.6 kcal·mol^{-1} and −35.4 kcal·mol^{-1} that in *n*-pentane and benzene, respectively, as shown in Fig. 2(a), (b), and (c). The more concentrated the negative charge, the easier to attract positively charged radicals to the site because of electrostatic inter-attraction.

When comparing the intermolecular interactions between BuLi and different solvents, it can be found that the maximum is 247.6 kcal·mol^{-1} in THF, whereas those of 210.2 kcal·mol^{-1} and 158.5 kcal·mol^{-1} are assigned to the systems in *n*-pentane and benzene, respectively, as shown in Fig. 2(d), (e) and (f). The ESP is strongly related to the ΔE_{els} (Fig. 1(c), (f)), whereas intermolecular interactions are related to the ΔE_{disp} (Fig. 1(c), (f)) [49]. What is more, the number of charged electrons of Li atom in BuLi in different solvents was calculated separately using the atomic dipole corrected Hirshfeld atomic charge (ADCH) method. In the gas phase, the number of electrons on the Li atom is 0.65 e and the number of charged electrons decreases with increasing solvent polarity. This indicates that electrons are transferred from the Li atom to the solvent, with more electrons transferred corresponding to stronger solvation.

3.2. Energy insights into the initiation mechanism of St in different solvents

The initiation energy barriers of St in different solvents were calculated by DFT calculations, as shown in Fig. 3. When comparing the Gibbs free energies of BuLi in different solvents, the lowest one is observed in THF. This is consistent with the conclusions obtained in Figs. 1 and 2 that THF interacts more strongly with BuLi, therefore BuLi is most stable in THF. It can be found that the initiation energy barrier in Fig. 3 is the largest in THF, *i.e.*, 37.80 kcal·mol^{-1} (in THF) > 35.86 kcal·mol^{-1} (in benzene) > 35.27 kcal·mol^{-1} (in *n*-pentane). The results show that the stronger the solvent polarity, the higher the monomer initiation energy barrier. In addition, we also calculated the chain propagation energy barriers of St in different solvents (Fig. S1). Calculations revealed that the energy barrier for the anionically active species in THF to propagate as free ions is 12.13 kcal·mol^{-1}, which is much lower than the energy barrier (34.65 kcal·mol^{-1}) as ion pairs, as shown in Fig. S1(c). By comparison, only the active species propagates as ion pairs in both *n*-pentane and benzene. Detailed information can be referred to Supplementary Material.

From a thermodynamic perspective, the probability of BuMLi generation is contingent on the free energy barrier, which is closely associated with ambient temperature. We calculated the free energy barriers of the transition state under different solvents, represented as $\Delta G_{TS-Benzene}$ (kcal·mol^{-1}), $\Delta G_{TS-n-Pentane}$ (kcal·mol^{-1}), and ΔG_{TS-THF} (kcal·mol^{-1}), respectively, to illustrate the thermodynamic nature of the BuMLi generation, as shown in Fig. 4(a). It can be observed that the free energy barriers follow the same trend in different solvents. In contrast to most chemical reactions, the initiation reaction is more favorable at lower temperature. Further exploring the origin of Gibbs free energy changes at different temperatures, ΔH_{TS-THF} (kcal·mol^{-1}) and $-T\Delta S_{TS-THF}$ (kcal·mol^{-1}) were calculated, as shown in Fig. 4(b). ΔH_{TS-THF} does not vary significantly with temperature, whereas $-T\Delta S_{TS-THF}$ shows an increasing trend. It can hence be introduced that ΔS_{TS-THF} (kcal·mol^{-1}·K^{-1}) decreases with temperature increasing, probably because it is more difficult for the solvent to stabilize this transition state at low temperature.

3.3. Kinetic understanding of LAP in different solvents

The logarithmic kinetic plots in the three solvents for different initiator and monomer concentrations are given in Fig. 5. The simulated curves for $[(BuLi)_{n\ =\ 6,4,1}]$:[M] = 0.003:0.715 conditions were validated by the experimental data from Refs. [16,17]. The polymerization rates of LAP in the three solvents increase with the increase in initiator concentration, as shown in Fig. 5(a), (b), and (c), which is due to the increase in the concentration of the anionic active species in the system. With increasing monomer concentration, the slope of the logarithmic kinetic plot is found to increase only in THF, while no change in polymerization rate with different monomer concentrations in benzene and *n*-pentane, as shown in Fig. 5(d), (e) and (f). These results indicate that the kinetic behavior in THF differs from that in either benzene or *n*-pentane. Specifically, the LAP in benzene or *n*-pentane allows the polymerizations to follow the first-order kinetic feature toward monomer propagation (Eq. (8)).

$$R_P = -\frac{d[M]}{dt} = k_{pi}[BuM_n^-Li^+][M] \quad (8)$$

$$R_P = -\frac{d[M]}{dt} = k_{pi}[BuM_n^-Li^+][M] + k_p[BuM_n^-][M] \quad (9)$$

where the R_P (mol·L^{-1}·s^{-1}) is the polymerization rate, $[BuM_n^-Li^+]$ (mol·L^{-1}) is the ion pair concentration, $[BuM_n^-]$ (mol·L^{-1}) is the free ion concentration, k_{pi} (L·mol^{-1}·s^{-1}) is the propagation rate

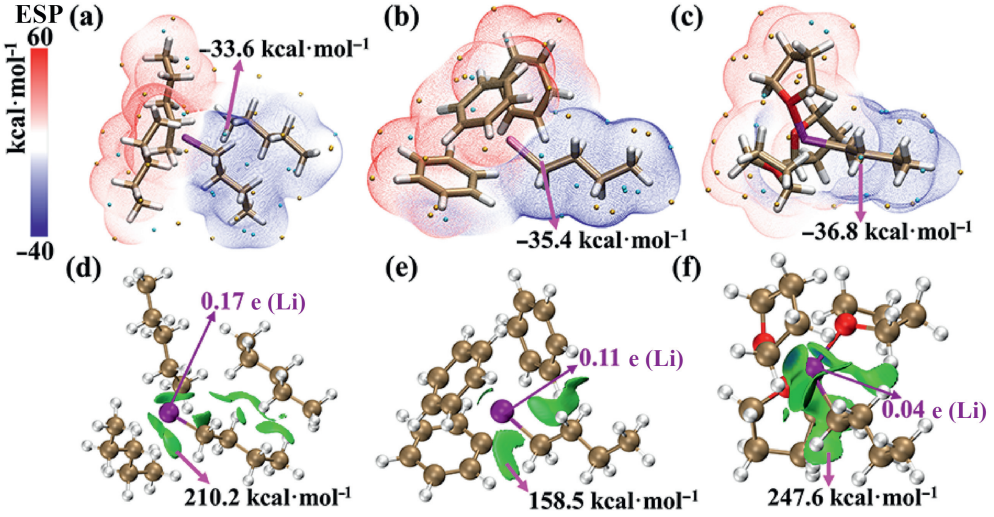

Fig. 2. Color-mapped isosurface graph of electrostatic potential (ESP) of BuLi and different solvents. Visualized independent gradient model based on the Hirshfeld partition (IGMH) analysis of BuLi and different solvents. In particular, the green part indicates vdW interactions; the blue part indicates strong intramolecular interactions. (a) and (d) BuLi in *n*-pentane, (b) and (e) BuLi in benzene, (c) and (f) BuLi in THF.

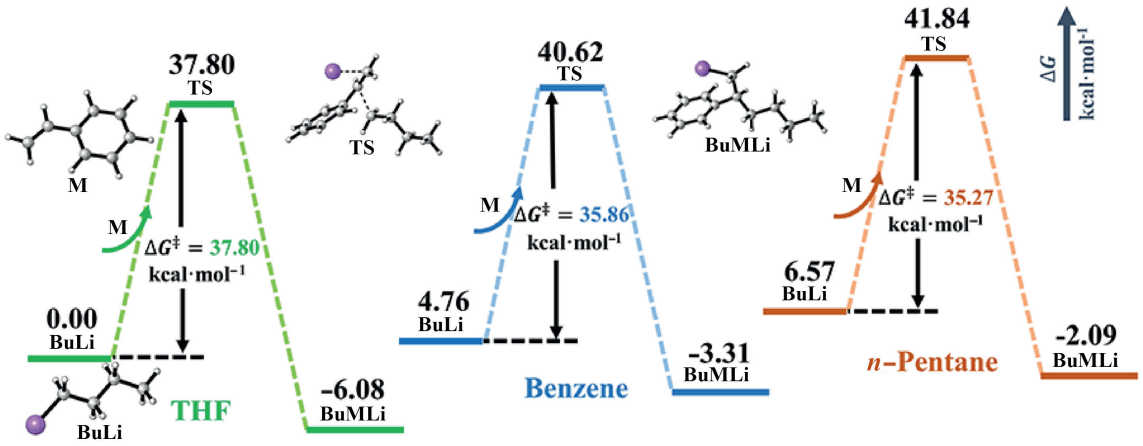

Fig. 3. Computed energy profiles of St initiation in different solvents at 298.15 K.

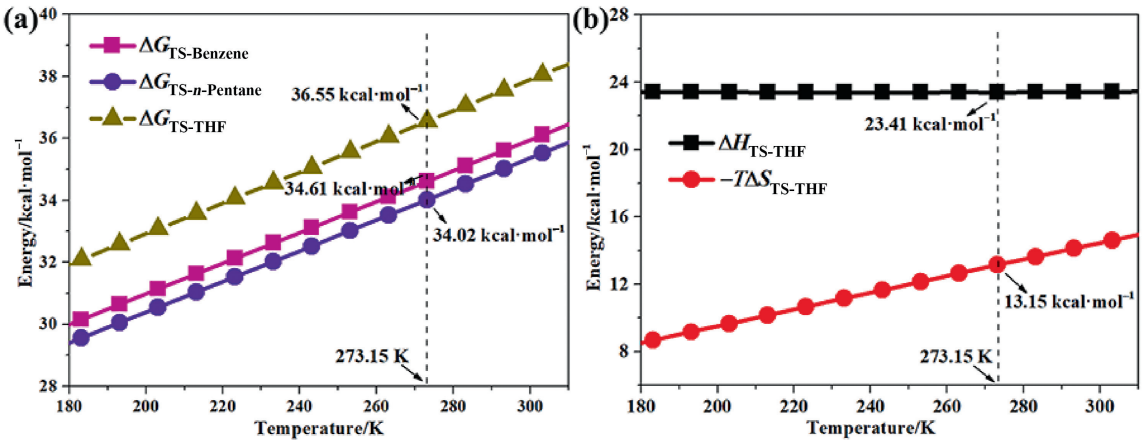

Fig. 4. (a) Temperature-dependent $\Delta G_{TS-Benzene}$, $\Delta G_{TS-n-Pentane}$, and ΔG_{TS-THF} during the formation of BuMLi. (b) Temperature-dependent ΔH_{TS-THF}, and $-T\Delta S_{TS-THF}$ during the formation of BuMLi in THF.

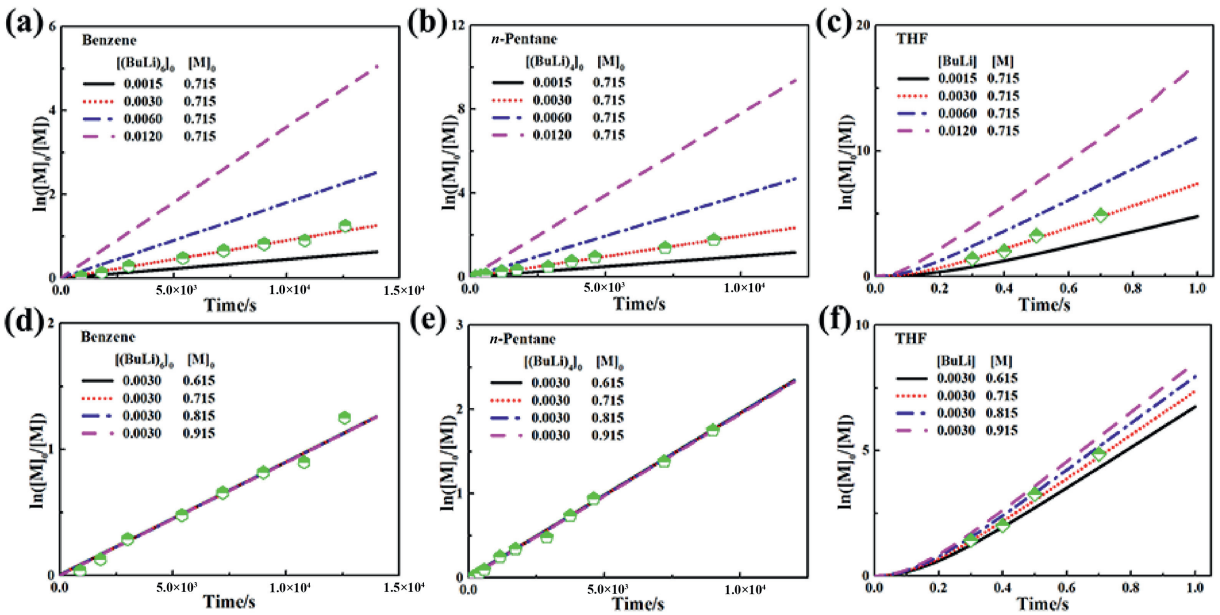

Fig. 5. Simulation results of the kinetics of LAP in different solvents at 298.15 K: (a), (b) and (c) semilogarithmic kinetic plots for different initiator concentrations; (d) (e) and (f) semilogarithmic kinetic plots for different monomer concentrations with constant total volume. The experimental data come from Refs. [16,17].

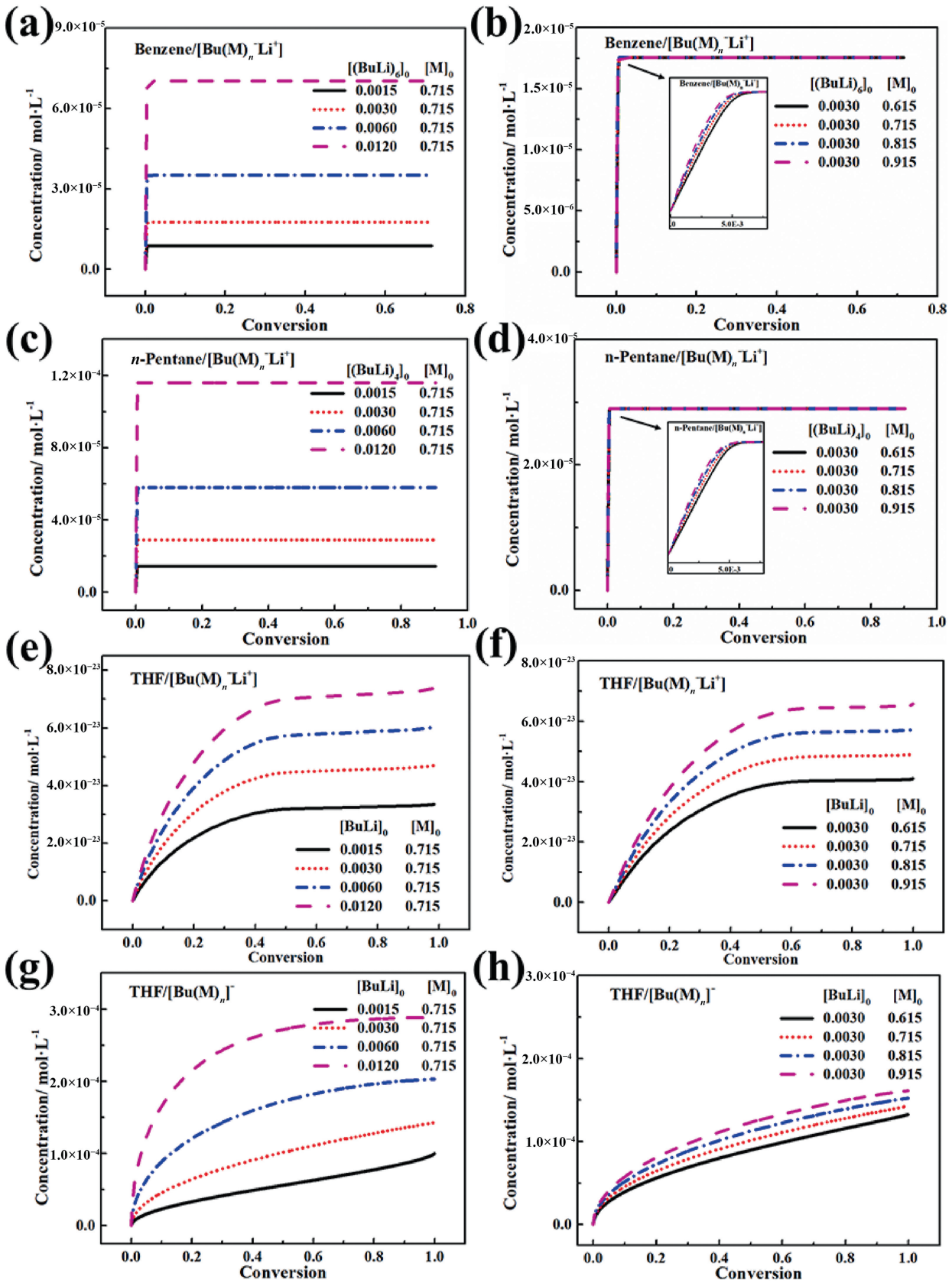

Fig. 6. Simulation results of the variations of anionic active species concentration with conversion in different solvents: (a), (c), (e) and (g) results at different initiator concentrations; (b), (d), (f) and (h) results at different monomer concentrations.

coefficient of the [$BuM_n^-Li^+$] and k_p ($L\cdot mol^{-1}\cdot s^{-1}$) is the propagation rate coefficient of the [BuM_n^-].

In contrast, the kinetics of LAP in THF exhibit an induction period followed by fast propagation. A weak curvature can be observed for the semilogarithmic kinetic plots in Fig. 5(f), indicating the effect of THF on LAP, which is different from the first-order kinetics of the LAP of St in benzene (Fig. 5(d)). Interestingly, such bending is also found in the cationic ring-opening polymerization of 2-oxazolines [50]. Here, it can be considered that the polymerization rate is determined by a combination of ion pairs [$BuM_n^-Li^+$] and free ions [BuM_n^-] (Eq. (9)). Since k_p is much larger than k_{pi}, the propagation of monomers in THF is dominated by free ions [BuM_n^-].

To further explore the underlying mechanism, the variations of anionic active species concentration with conversion at different initiator concentrations are shown in Fig. 6(a), (c), (e) and (g). In benzene and *n*-pentane, the concentration of [$BuM_n^-Li^+$] reaches equilibrium at a very low conversion, leading to fast propagation. In THF, both concentrations of [$BuM_n^-Li^+$] and [BuM_n^-] increase slowly with the conversion, which is attributed to the presence of an induction period.

Similarly, the variations of anionic active species concentration with the conversion at different monomer concentrations were tracked, as shown in Fig. 6(b), (d), (f) and (h). It can be found that in benzene and *n*-pentane, the concentration of anionically active species [$BuM_n^-Li^+$] reaches equilibrium at a lower monomer conversion of about 0.5%. Given that, $k_{pi}\cdot$[$BuM_n^-Li^+$] can be considered as constant, and thus monomer concentration shows almost no influence on the logarithmic kinetic plot. While in THF, both concentrations of [$BuM_n^-Li^+$] and [BuM_n^-] continue to increase gradually. Therefore, the higher the monomer concentration is, the shorter the induction period will be. In addition, the concentration of free ion active species [BuM_n^-] in THF is much larger than that of ion pairs [$BuM_n^-Li^+$] throughout the whole polymerization, confirming the dominant role of free ion active species in propagation in THF.

4. Conclusions

In this work, the effect of solvents on the LAP of St was investigated by computational simulations, including the mechanism by DFT calculations and MoM-based kinetic modeling. Firstly, the dominant reason for the lower interaction energy in the stronger polarity solvent is due to the electrostatic interaction energy through energy decomposition analysis. Furthermore, electrons are transferred from the Li atom to the solvent molecule, with more electrons transferring corresponding to the stronger solvation through electrostatic potential and intermolecular interactions analysis. In terms of the initiation mechanism, we found that the stronger the solvent polarity, the higher the monomer initiation energy barrier and the smaller the initiation rate coefficient. From a thermodynamic perspective, the reaction is more favorable at lower temperatures, probably because it is more difficult for the solvent to stabilize the transition state at low temperatures.

In addition, the kinetic models corresponding to three different solvents were established based on the method of moments with the rate coefficients determined by DFT calculations and TST theory. It is found that in benzene and *n*-pentane, the polymerization rates show first-order kinetic for monomers under different initiator and monomer concentrations. By contrast, slow initiation and fast propagation are exhibited in THF. An in-depth examination of the variations of the concentration of active anionic species [$BuM_n^-Li^+$] under different conditions reveals that in benzene and *n*-pentane, the concentration of active species reaches equilibrium at a low monomer conversion. While in THF, the concentration of active species [BuM_n^-] shows a slowly increasing trend. This indicates a slow rate of free ion [BuM_n^-] formation, thus contributing to the slow initiation and fast propagation kinetic characteristics in THF. This computational study has deepened the understanding of the mechanism and kinetics of LAP considering the effect of solvents.

Declaration of Interest

The authors declare that they have no known competing financial interests or personal relationships that could have appeared to influence the work reported in this paper.

Acknowledgements

This work was financially supported by the National Natural Science Foundation of China (U21A20313, 22222807). The Center for high-performance Computing at Shanghai Jiao Tong University is also acknowledged.

Supplementary Material

Supplementary data to this article can be found online at https://doi.org/10.1016/j.cjche.2024.01.007.

Nomenclature

k_a	activation rate coefficient, s^{-1}
k_{da}	deactivation rate coefficient, $L\cdot mol^{-1}\cdot s^{-1}$
k_{in}	initiation rate coefficient, $L\cdot mol^{-1}\cdot s^{-1}$
k_p	free ion propagation rate coefficient, $L\cdot mol^{-1}\cdot s^{-1}$
k_{pi}	ion pair propagation rate coefficient, $L\cdot mol^{-1}\cdot s^{-1}$
k_1	disassociation rate coefficient for butyllithium aggregates, s^{-1}
k_{-1}	association rate coefficient for butyllithium, $L^5\cdot mol^{-5}\cdot s^{-1}$ in benzene and $L^3\cdot mol^{-3}\cdot s^{-1}$ in *n*-pentane

References

[1] M. Szwarc, 'Living' polymers, *Nature* 178 (4543) (1956) 1168–1169.
[2] A. Hirao, R. Goseki, T. Ishizone, Advances in living anionic polymerization: From functional monomers, polymerization systems, to macromolecular architectures, *Macromolecules* 47 (6) (2014) 1883–1905.
[3] R.B. Grubbs, R.H. Grubbs, 50th anniversary perspective: Living polymerization—Emphasizing the Molecule in Macromolecules, *Macromolecules* 50 (18) (2017) 6979–6997.
[4] P.W. Liu, J.G. Du, Y.T. Ma, Q.Y. Wang, K.H. Lim, B.G. Li, Progress of polymer reaction engineering: From process engineering to product engineering, *Chin. J. Chem. Eng.* 50 (2022) 3–11.
[5] Y.N. Zhou, J.J. Li, T.T. Wang, Y.Y. Wu, Z.H. Luo, Precision polymer synthesis by controlled radical polymerization: Fusing the progress from polymer chemistry and reaction engineering, *Prog. Polym. Sci.* 130 (2022) 101555.
[6] E. Farkas, Z.G. Meszena, A.F. Johnson, Molecular weight distribution design with living polymerization reactions, *Ind. Eng. Chem. Res.* 43 (23) (2004) 7356–7360.
[7] L. Xie, L.T. Zhu, Z.H. Luo, Computational fluid dynamics simulation of multiscale mixing in anionic polymerization tubular reactors, *Chem. Eng. Technol.* 39 (5) (2016) 857–864.
[8] E. Mastan, J.P. He, Continuous production of multiblock copolymers in a loop reactor: When living polymerization meets flow chemistry, *Macromolecules* 50 (23) (2017) 9173–9187.
[9] M. Szwarc, Living polymers. Their discovery, characterization, and properties, *J. Polym. Sci. Polym. Chem.* 36 (1) (1998) ix–xv.
[10] C. Carvajal, K.J. Tölle, J. Smid, M. Szwarc, Studies of solvation phenomena of ions and ion pairs in dimethoxyethane and tetrahydrofuran, *J. Am. Chem. Soc.* 87 (24) (1965) 5548–5553.
[11] Y.N. Zhou, J.J. Li, Y.Y. Wu, Z.H. Luo, Role of external field in polymerization: Mechanism and kinetics, *Chem. Rev.* 120 (5) (2020) 2950–3048.
[12] D. Baskaran, Strategic developments in living anionic polymerization of alkyl (meth)acrylates, *Prog. Polym. Sci.* 28 (4) (2003) 521–581.
[13] S.D. Robertson, M. Uzelac, R.E. Mulvey, Alkali-metal-mediated synergistic effects in polar main group organometallic chemistry, *Chem. Rev.* 119 (14) (2019) 8332–8405.

[14] X.R. Zheng, Z.H. Xi, L. Zhao, Solvent strategy toward living cationic polymerization of trichloro(*N*-silyl)phosphoranimine based on Density Functional Calculations and experimental verification, *Chem. Eng. J.* 377 (2019) 120004.
[15] C. Hahn, M. Rauschenbach, H. Frey, Merging styrene and diene structures to a cyclic diene: Anionic polymerization of 1-vinylcyclohexene (VCH), *Angew. Chem. Int. Ed.* 62 (28) (2023) e202302907.
[16] D.J. Worsfold, S. Bywater, Anionic polymerization of styrene, *Can. J. Chem.* 38 (10) (1960) 1891–1900.
[17] S. Bywater, D.J. Worsfold, Anionic polymerization of styrene effect of tetrahydrofuran, *Can. J. Chem.* 40 (8) (1962) 1564–1570.
[18] H. Morita, M. Van Beylen, The mechanism of the propagation in the anionic polymerization of polystyryllithium in non-polar solvents elucidated by density functional theory calculations. A study of the negligible part played by dimeric ion-pairs under usual polymerization conditions, *Polymers* 11 (6) (2019) 1022.
[19] T. Takagi, T. Toda, M. Miya, K. Takenaka, DFT study on the anionic polymerization of phenyl-substituted[3]dendralene derivatives: Reactivities of monomer and chain end carbanion, *Polym. J.* 54 (5) (2022) 643–652.
[20] T.E. Long, H.Y. Liu, B.A. Schell, D.M. Teegarden, D.S. Uerz, Determination of solution polymerization kinetics by near-infrared spectroscopy. 1. Living anionic polymerization processes, *Macromolecules* 26 (23) (1993) 6237–6242.
[21] E. Rieger, T. Gleede, K. Weber, A. Manhart, M. Wagner, F.R. Wurm, The living anionic polymerization of activated aziridines: A systematic study of reaction conditions and kinetics, *Polym. Chem.* 8 (18) (2017) 2824–2832.
[22] K.F. O'Driscoll, A.V. Tobolsky, Kinetics of anionic polymerization of styrene, *J. Polym. Sci.* 35 (128) (1959) 259–265.
[23] F.S. Dainton, K.J. Ivin, R.T. LaFlair, Kinetics of anionic polymerization of styrene in tetrahydropyran, *Eur. Polym. J.* 5 (3) (1969) 379–386.
[24] A.V. Yakimansky, A.H.E. Müller, M. van Beylen, Density functional theory study on the aggregation and dissociation behavior of lithium chloride in THF and its interaction with the active centers of the anionic polymerization of methyl methacrylate and styrene, *Macromolecules* 33 (15) (2000) 5686–5692.
[25] O. Tai, R. Hopson, P.G. Williard, Aggregation and solvation of *n*-butyllithium, *Org. Lett.* 19 (15) (2017) 3966–3969.
[26] M.P. Crockett, J. Piña, A.R. Gogoi, R.F. Lalisse, A.V. Nguyen, O. Gutierrez, A.A. Thomas, Breaking the *tert*-butyllithium contact ion pair: A gateway to alternate selectivity in lithiation reactions, *J. Am. Chem. Soc.* 145 (19) (2023) 10743–10755.
[27] D. Margerison, J.P. Newport, Degree of association of *n*-butyl lithium in hydrocarbon media, *Trans. Faraday Soc.* 59 (1963) 2058–2063.
[28] D.R. D'hooge, P.H.M. Van Steenberge, M.F. Reyniers, G.B. Marin, The strength of multi-scale modeling to unveil the complexity of radical polymerization, *Prog. Polym. Sci.* 58 (2016) 59–89.
[29] T. Qin, Z.H. Xi, L. Zhao, W.K. Yuan, Monte Carlo simulation of sequential structure control of AN-MA-IA aqueous copolymerization by different operation modes, *Chin. J. Chem. Eng.* 46 (2022) 231–242.
[30] M. Edeleva, P.H.M. Van Steenberge, M.K. Sabbe, Connecting gas-phase computational chemistry to condensed phase kinetic modeling: The state-of-the-art, *Polymers* 13 (18) (2021) 3027.
[31] S. Li, C. Bian, Z.X. Liu, Y.N. Zhou, Z.H. Luo, Identifying the essential roles of light and sonication in dual-stimuli regulated bulk atom transfer radical polymerization by multiscale simulation, *AIChE J.* 69 (10) (2023) e18155.
[32] C. Bian, S. Li, N.T. Yang, H. Chen, W. Feng, Y.N. Zhou, Z.H. Luo, In-depth mechanistic and kinetic investigation of sonochemically mediated atom transfer radical polymerization using modeling approach, *Chem. Eng. J.* 464 (2023) 142642.
[33] M.J. Frisch, G.W. Trucks, H.B. Schlegel, G.E. Scuseria, M.A. Robb, J.R. Cheeseman, G. Scalmani, V. Barone, G.A. Petersson, H. Nakatsuji, X. Li, M. Caricato, A. V. Marenich, J. Bloino, B.G. Janesko, R. Gomperts, B. Mennucci, H.P. Hratchian, J.V. Ortiz, A.F. Izmaylov, J.L. Sonnenberg, D. Williams-Young, F. Ding, F. Lipparini, F. Egidi, J. Goings, B. Peng, A. Petrone, T. Henderson, D. Ranasinghe, V. G. Zakrzewski, J. Gao, N. Rega, G. Zheng, W. Liang, M. Hada, M. Ehara, K. Toyota, R. Fukuda, J. Hasegawa, M. Ishida, T. Nakajima, Y. Honda, O. Kitao, H. Nakai, T. Vreven, K. Throssell, J.A. Montgomery Jr., J.E. Peralta, F. Ogliaro, M.J. Bearpark, J.J. Heyd, E.N. Brothers, K.N. Kudin, V.N. Staroverov, T.A. Keith, R. Kobayashi, J. Normand, K. Raghavachari, A.P. Rendell, J.C. Burant, S.S. Iyengar, J. Tomasi, M. Cossi, J.M. Millam, M. Klene, C. Adamo, R. Cammi, J.W. Ochterski, R.L. Martin, K. Morokuma, O. Farkas, J.B. Foresman, D.J. Fox, Gaussian 16 Rev. A.03, 2016. Wallingford, CT.
[34] A.V. Marenich, C.J. Cramer, D.G. Truhlar, Performance of SM6, SM8, and SMD on the SAMPL1 test set for the prediction of small-molecule solvation free energies, *J. Phys. Chem. B* 113 (14) (2009) 4538–4543.
[35] T. Lu, Q.X. Chen, Shermo: A general code for calculating molecular thermochemistry properties, *Comput. Theor. Chem.* 1200 (2021) 113249.
[36] S. Boresch, F. Tettinger, M. Leitgeb, M. Karplus, Absolute binding free energies: A quantitative approach for their calculation, *J. Phys. Chem. B* 107 (35) (2003) 9535–9551.
[37] H. Eyring, The activated complex in chemical reactions, *J. Chem. Phys.* 3 (2) (1935) 107–115.
[38] C. Doubleday, R. Armas, D. Walker, C.V. Cosgriff, E.M. Greer, Heavy-atom tunneling calculations in thirteen organic reactions: Tunneling contributions are substantial, and Bell's formula closely approximates multidimensional tunneling at ≥250 K, *Angew. Chem., Int. Ed.* 56 (42) (2017) 13099–13102.
[39] T. Lu, F.W. Chen, Multiwfn: a multifunctional wavefunction analyzer, *J. Comput. Chem.* 33 (5) (2012) 580–592.
[40] W. Humphrey, A. Dalke, K. Schulten, VMD: Visual molecular dynamics, *J. Mol. Graph.* 14 (1) (1996) 33–38, 27–28.
[41] T. Lu, Q.X. Chen, Simple, efficient, and universal energy decomposition analysis method based on dispersion-corrected density functional theory, *J. Phys. Chem. A* 127 (33) (2023) 7023–7035.
[42] E. Mastan, S.P. Zhu, Method of moments: A versatile tool for deterministic modeling of polymerization kinetics, *Eur. Polym. J.* 68 (2015) 139–160.
[43] Y.N. Zhou, Z.H. Luo, State-of-the-art and progress in method of moments for the model-based reversible-deactivation radical polymerization, *Macromol. React. Eng.* 10 (6) (2016) 516–534.
[44] D.R. D'Hooge, M.F. Reyniers, G.B. Marin, Methodology for kinetic modeling of atom transfer radical polymerization, *Macromol. React. Eng.* 3 (4) (2009) 185–209.
[45] J. Liu, T.T. Wang, Z.H. Luo, Y.N. Zhou, *In silico* mechanically mediated atom transfer radical polymerization: A detailed kinetic study, *AIChE J.* 67 (5) (2021) e17151.
[46] Y.Y. Wu, F.L. Figueira, M. Edeleva, P.H.M. Van Steenberge, D.R. D'Hooge, Y.N. Zhou, Z.H. Luo, Cost-efficient modeling of distributed molar mass and topological variations in graft copolymer synthesis by upgrading the method of moments, *AIChE J.* 68 (4) (2022) e17559.
[47] P. Deglmann, I. Müller, F. Becker, A. Schäfer, K.D. Hungenberg, H. Weiß, Prediction of propagation rate coefficients in free radical solution polymerization based on accurate quantum chemical methods: Vinylic and related monomers, including acrylates and acrylic acid, *Macromol. React. Eng.* 3 (9) (2009) 496–515.
[48] V. Aviyente Değirmenci, V. Van Speybroeck, M. Waroquier, DFT study on the propagation kinetics of free-radical polymerization of α-substituted acrylates, *Macromolecules* 42 (8) (2009) 3033–3041.
[49] T. Lu, Q.X. Chen, Independent gradient model based on Hirshfeld partition: A new method for visual study of interactions in chemical systems, *J. Comput. Chem.* 43 (8) (2022) 539–555.
[50] M. Glassner, D.R. D'hooge, J.Y. Park, P.H.M. Van Steenberge, B.D. Monnery, M. F. Reyniers, R. Hoogenboom, Systematic investigation of alkyl sulfonate initiators for the cationic ring-opening polymerization of 2-oxazolines revealing optimal combinations of monomers and initiators, *Eur. Polym. J.* 65 (2015) 298–304.